ARCHIVES of
Computational Materials Science and Surface Engineering

International Scientific Journal
published quarterly by the Association of Computational Materials Science and Surface Engineering

2009 • Volume 1 • Issue 4 • 213-224

Determination of wetting at elevated temperatures using image analysis

D. Kocaefe*, G. Ergin, V. Villeneuve, Y. Kocaefe
Department of Applied Sciences, University of Quebec at Chicoutimi 555 boul.
De l'Université Chicoutimi, Québec, G7H 2B1, Canada
* Corresponding author: E-mail address: dkocaefe@uqac.ca

Received in a revised form 20.08.2008

ABSTRACT

Purpose: Wettability of a solid by a liquid is characterized by the contact angle or the wettability parameter which is a function of the contact angle and the surface tension. One well-known method to determine the contact angle and the surface tension experimentally is the sessile-drop method. The accuracy of this method depends on different geometric parameters measured from the image of the liquid drop on the solid captured during the experiments. In this study, software was developed to measure the parameters required for the calculation of the contact angle and the surface tension as well as all other relevant parameters such as spreading and drop volume from the sessile-drop images.

Design/methodology/approach: The image analysis program presented in this study was developed to determine the wetting characteristics of a solid/molten metal system at elevated temperatures; hence, it deals mainly with the measurement of the contact angle and the calculation of the surface tension from the images captured during such experiments.

Findings: In this study, a robust image analysis program has been developed. It gives not only the contact angle and the surface tension, but also a number of other important parameters of interest in wetting such as the spreading and the change in the surface area and volume of the sessile drop under different lighting conditions.

Practical implications: The future work will cover the development of new filters which will eliminate further the interference of components placed outside the "analysis window" with the components to be analyzed. This task will have an impact at the level of filtration in the operation pipeline presented above.

Originality/value: The results are validated by comparing them with the measurements conducted using an optical microscope; and the agreement is good.

Keywords: Wetting; Contact angle; Surface tension; Molten metal; High temperature

Reference to this paper should be given in the following way:

D. Kocaefe, G. Ergin, V. Villeneuve, Y. Kocaefe, Determination of wetting at elevated temperatures using image analysis, Archives of Computational Materials Science and Surface Engineering 1/4 (2009) 213-224.

METHODS OF ANALYSIS AND MODELLING

1. Introduction

The wetting phenomenon plays an important role in many industrial processes such as metal-matrix composite production, joining, metal filtration, and coating. When a liquid drop is placed on a solid surface, three interfaces form due to the presence of three phases (solid, liquid, and vapor). These interfaces occur at the boundaries of contact between the phases: solid/vapor, solid/liquid, and liquid/vapour; and they meet at a point called the triple point. A force balance at the triple point determines the

wettability of the solid phase by the liquid phase in the presence of a given vapor phase.

In some processes, the enhanced wetting along the solid/liquid interface is preferred since the quality of the final product is improved (e.g. better quality composites, joints with superior mechanical properties, increased efficiency in metal filtration, and coatings with enhanced adherences). On the contrary, in some applications, non-wetting characteristics are preferred to prevent the undesirable interactions between the solid and the liquid. For example, if a hot metal does not wet the wall of its container, the corrosion of the container and the contamination of the metal are significantly reduced. Therefore, to control better some of the industrial processes and the quality of their products, wetting characteristics of the relevant systems should be well understood. For this purpose, the chemical and physical interactions between the predominant phases (that is, the wetting phenomena taking place along the interfaces) should be determined.

The wetting phenomena can be described using the contact angle and/or the wettability parameter concepts. The contact angle, θ, is defined as the angle between the tangents drawn to the solid/vapor and liquid/vapor interfaces (see Figure 1). This figure also shows the interfacial tensions between different phases: solid/vapour (γ^{SV}), solid/liquid interfaces (γ^{Sl}), and liquid/vapor (γ^{lv}). The interfacial tension γ^{lv} is usually called the surface tension. The wettability parameter, which is defined as $\gamma^{lv}\cos(\theta)$, is product of the surface tension and the cosine of the contact angle. The system is considered wetting when the contact angle is less than 90°. In this case, the wettability parameter ($\gamma^{lv}\cos\theta$) is greater than zero, and the degree of wettability increases as θ approaches zero. If the contact angle is greater than 90°, the system is non-wetting, and the wettability parameter has a negative value. As the contact angle approaches 180°, the wettability decreases.

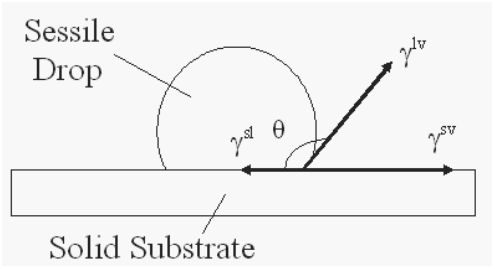

Fig. 1. A liquid sessile drop in contact with a solid substrate

Since the wettability can be measured in terms of the contact angle and/or the wettability parameter, the precise measurement of the contact angle and the surface tension is crucial. The image analysis program presented in this study was developed to determine the wetting characteristics of a solid/molten metal system at elevated temperatures; hence, it deals mainly with the measurement of the contact angle and the calculation of the surface tension from the images captured during such experiments. This is a unique situation. At elevated temperatures, the metal drop as well as all the other experimental system components within the furnace becomes red. In addition, the intensity of the color varies depending on the experimental conditions, especially the temperature. Therefore, it is difficult to separate the drop from its surroundings in order to carry out the desired measurements using the image analysis technique. Most of the commercially available codes fail to determine the wetting parameters because the system lighting is very different than the other more common sessile-drop applications. The software developed in this work fills this void.

Numerous techniques have been developed to measure the surface tension and/or the contact angle such as the Du Nouy ring method, the Wilhelmy plate method, the spinning drop method, the pendant drop method, the bubble pressure method, the drop volume method, the Washburn method, and the sessile drop method [1,15]. The descriptions of all these methods can be found elsewhere [1,15], and most of these techniques are used for measurements at low temperatures since many products are designed for consumption at ambient temperature. More than 80% of the wetting studies at elevated temperatures are carried out using the sessile drop method [8], and thus this method was chosen for the current study in which the experiments were conducted above 700ºC.

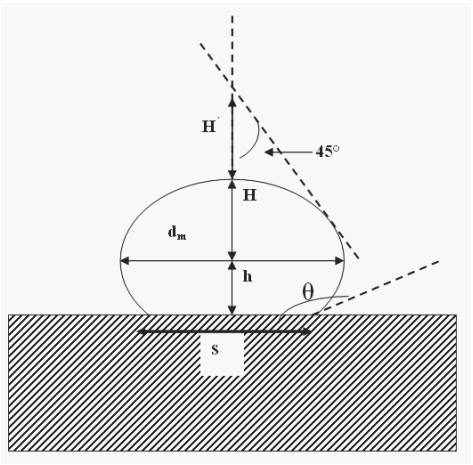

Fig. 2. Geometric factors measured for a liquid drop in contact with a solid substrate for the salculation of surface tension [14]

Fundamentally, the sessile drop represents a special case of the capillary phenomena; thus the surface tension can be found by solving the Laplace equation governing the shape of the macroscopic menisci [14]. Bashford and Adams [5] solved this equation and prepared tables from which it is possible to calculate the surface tension if certain geometric dimensions of the sessile drop given in Fig. 2 are known. Similar tables were prepared by Koshevnik et al. [11] for the calculation of the surface tension using the sessile drop profiles. In the current study, the surface tension of the molten metal under an argon atmosphere at 730°C was calculated using the empirical relationship given by Dorsey [7] :

$$\gamma^{lv} = \frac{g\rho_L d_m^2}{4}\left(\frac{0.0520}{f} - 0.1227 + 0.0481\right) \quad (1)$$

$$f = \left(\frac{2H'}{d_m}\right) - 0.4142$$

where γ^{lv} is the surface tension, ρ_L is the liquid density, and g is the gravitational acceleration. d_m is the diameter of the largest section of the drop, and H' is the distance between the top of the drop and the intersection of the vertical line with the 45° tangent line as shown in Fig. 2. If d_m and H' can be measured from the image, the surface tension can be calculated. The accuracy of the measurements is very important. A small error in dimensions affects the surface tension significantly. Equation (1) gives quite accurate results and is used for the surface tension calculations. Then again, if desired, any other empirical equation can be incorporated into the image analysis software.

Various methods based on the sessile drop shape analysis have been reported in the literature to calculate the contact angle. Some of the methods are based on the drop outlines obtained using singular points [19]. Others fit different functions to the drop profiles such as a polynomial [6,13] or an ellipsoid [18]; in some cases, a least square fit is carried out [18]. The triple point is found from the intersection of the baseline and the drop profile by solving the corresponding equations simultaneously. The contact angle is calculated from the slope of these equations around the triple point. Others use the theoretical knowledge of the drop shape (such as the Laplacian axisymmetric drop) which involves the solution of capillary equations [16,17,18]. Then, the contact angles from these profiles are found through certain numerical solutions of the governing differential equations. Some use image analysis to obtain the drop profiles [2,18,22] then fit an expression to these profiles to calculate the contact angle and the surface tension. In this work, the contact angles are determined directly from the captured images of the sessile drop by using the image analysis program explained in detail in the following sections.

In this study, a robust image analysis program has been developed. It gives not only the contact angle and the surface tension, but also a number of other important parameters of interest in wetting such as the spreading and the change in the surface area and volume of the sessile drop under different lighting conditions. If the wetting is chemical in nature, the length of the interface between the solid and the liquid drop will change with time. This behavior is known as the spreading. The change in the length of the interface can be followed during the experiment using the image analysis program. Also, the change of the surface area and, consequently, the volume of the drop can be deduced from the image analysis. If the solid is porous or granular, the liquid metal might penetrate into the solid. The amount of liquid that has penetrated into the solid can be found if the change in the area of the drop is followed with time. If one or more of the alloying elements vaporize due to their high vapor pressures at elevated temperatures, the size of the sessile drop changes. This change in size can also be measured by the program.

The set-up for the sessile drop experiments is shown schematically in Figure 3. An injection chamber and a sample crucible with three compartments are placed inside an Inconnel tube, which is heated by a horizontal electric furnace. The injection chamber contains the metal sample. The solid substrate is put in the middle compartment of the sample crucible; and titanium particles are placed in the other two compartments. The titanium particles in the vicinity of the sessile drop minimize the oxidation of the sessile drop at high temperatures. The experiments are conducted under an argon atmosphere. Initially, vacuum is applied to the system which is, then, flushed with research grade argon gas. There are two lines supplying argon gas to the system. The line that is connected to the injection chamber is maintained at a slightly higher pressure than the main line. When the temperature in the furnace reaches the desired value, the metal is in liquid state in the injection chamber; then, it is pushed down onto the solid substrate by applying pressure. The images of the drop are captured through a quartz observation window using a digital camcorder. These images are analyzed for the measurement of the contact angle and the calculation of the surface tension. These analyses are explained in detail below.

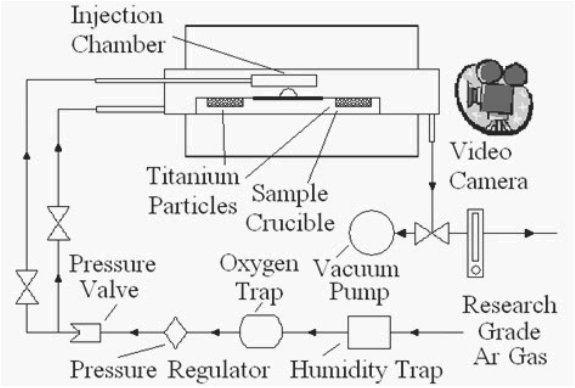

Fig. 3. A schematic view of the experimental sessile-drop system

2. Data acusation

The sessile drop experiments are recorded with a digital 3 chip CCD colour video camcorder (Canon, XL-1). The original images recorded are 768 pixels in width and 494 pixels in height. Afterwards, the video clip is transferred to a computer. A calibration method is incorporated into the software which calculates the actual dimensions of different entities (see Section 3 for details). This eliminates the necessity of placing the camera always at the same position and using always the same camera adjustments.

During the experiments, the short video clips are recorded onto the digital video cassettes. These clips are saved onto a hard disk by using the commercial video editing code CineStream® [23] in "mov" file format. Then, the format of the video is changed from "mov" to "avi" using the same commercial code. It is also possible to change the format from "mov" to "mpg" using a shareware program called TMPGEnc. The change in format of the short clip makes the data storage much easier. For example, a video clip of 5 minutes and 18 seconds requires 1.2 GB space in "mov" file format; however, the same video clip takes up 61.6 MB space in "avi" file format and 62.6 MB space in "mpg" file format. While the video clip is being recorded, the images are saved at a rate of 29.97 frames per second. Using the same video editing code, it is also possible to convert these video clips into image sequences in "bmp" and "jpg" file formats.

a)

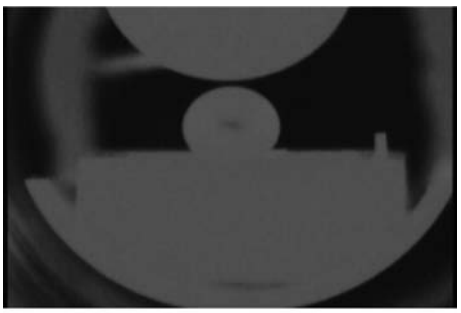

b)

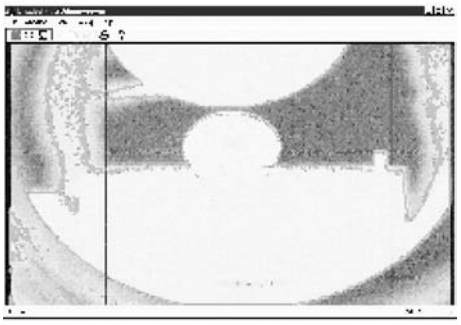

c)

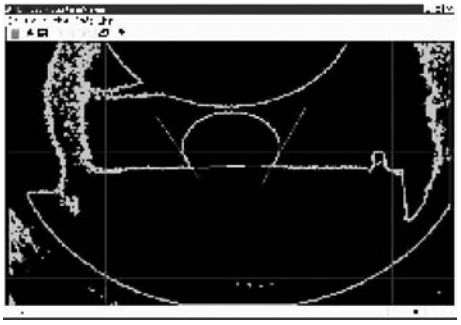

Fig. 4. Images from different phases of the image analysis program: (a) Raw image from the experiment, (b) Identification of the image outline by the image analysis program, c) determination of the contact angles by the image analysis program

The standard adopted within the framework of this project is the "bmp" file format because of the simplicity of its structure and the availability of different commercial or shareware codes which can carry out the file conversion easily to this file format. Once the frames are converted to "bmp" file format (*bitmap image*) which is encoded with an image buffer depth of 24 bits, they constitute the input data of the image analysis software (Figure 4a). These files are not compressed. The typical resolution of each *bitmap image* is 720 pixels in width and 480 pixels in height. It should be noted that the slight reduction of the image resolution comes from the conversion process used. The image analysis program first identifies the outline of the objects (Figure 4b). Then, it measures the contact angles on both sides of the drop, calculates the parameters that are necessary for the surface tension calculations, and determines the surface area and the volume of the sessile drop as well as the length of the solid/liquid interface for the spreading (Figure 4c).

3. Software design

In this section, the analysis pipeline of the "drop analyser" software is presented. More detailed information on the development of each segment of the pipeline will be given in the following sections. The principal objective of the project is to measure the contact angle, θ, and to calculate the surface tension, γ^{lv}; this requires the measurement of the parameters H, H', h, and d_m that are shown on Fig. 2. In addition, the program should be able to measure the spreading, S, and calculate the volume of the drop as well. Therefore, it is necessary to identify correctly various patterns of the components in the image so that the desired properties of the pattern could be calculated.

The upper part of the solid substrate (rectangle) and the shape of the drop (circle or ellipse) have to be identified as two distinct patterns in order to measure the desired properties. In the rest of the text, the particle shape will be referred to as the circular component for simplicity; however, the drop can be either an ellipse or a circle. It should also be noted that these patterns do not necessarily have a perfect geometrical form. Imperfections can be found on the images of both the drop and the substrate. To remedy this, the contact angle is measured from both sides of the drop and an average is taken. Figure 5 presents an implantation diagram of the pipeline describing the image analysis software.

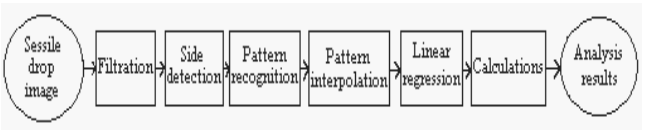

Fig. 5. Pipeline of operation in image analysis

The first two stages involve the processing of the input bitmap files. In the first stage, the image is transferred to the memory and a series of filters are applied. In the second stage, a new image containing the contour of the components is generated [3].

In the following two stages, a series of data structures grouping the contour pixels in subgroups called "patterns" are created. Three patterns are used for the images analyzed during this study. The first pattern represents the upper part of the sample crucible (solid substrate). The second and third patterns represent the circular components on both sides of the vertical axis (y-axis).

Calibration is another important stage of the software development. The SI unit system is used during all of the calculations; therefore, during the calibration, the dimension of one pixel is found in meters. The importance of the calibration lies in

the fact that placing the camera at slightly different positions in front of the quartz observation window may results in pixel size variation from one experiment to another. Two points of reference, based on any permanent component, must be defined to calculate the dimension of a pixel. Once the calibration is completed and the patterns are found, the calculation of the properties can be carried out using various numerical methods. In the following sections, each segment of the pipeline is described in more detail.

3.1. Filtration

The main objective of this segment is to prepare the image for the side detection algorithm. Since the intensity can be different from one experiment to another, an adjustment is necessary in order to clearly distinguish each component of the image. The technique used is called the "equalization by a color histogram" [11].

a)

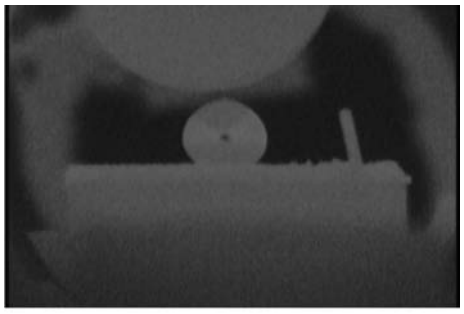

b)

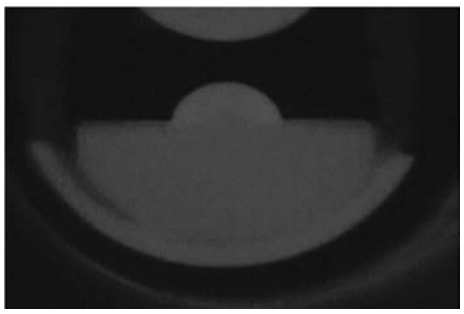

Fig. 6. Examples of template images showing the drop, substrate, and other parts of the furnace interior. (Red is the dominant color, and these images are taken one minute after the contact): a) non-wetting case: aluminium on alumina, b) wetting case: aluminium-magnesium alloy on fused silica

In this technique, first a histogram of colors found in the image is created. Due to the high temperatures involved during the actual experiments, the drop and the substrate radiate in the same range of frequency, and the colors have a tendency to regroup. Figures 6a and 6b show examples of the initial images obtained during the experiments for non-wetting and wetting systems, respectively. As it can be seen from these figures, red is the dominant color. An example of the color distribution histogram is shown in Figure 7a.

a)

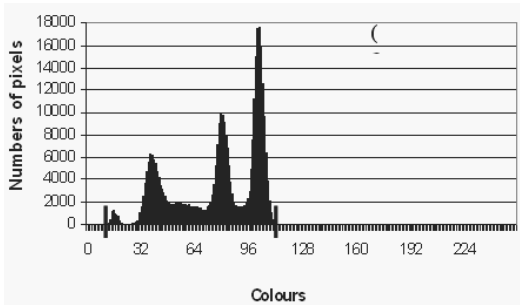

b)

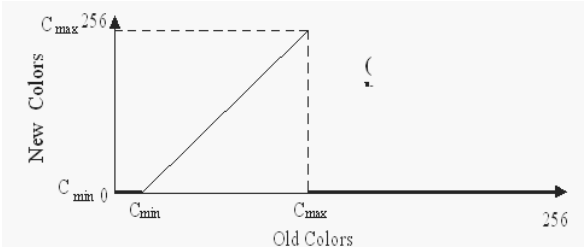

Fig. 7. Readjustment of the colors for the components of interest: a)histogram of the color distribution before modification and the coefficient of active color window, b) color conversion

In order to separate the desired components of the image from the rest which are not of interest (noise), first a modification of the color intensity is carried out. From the histogram, the minimum and maximum colors of the desired components are identified. Figure 7a shows a typical histogram. Taking these two known values as the limits, a filter is used to modify the colors as shown in Figure 7b. Therefore, a troublesome step according to many studies in the literature [4] the noise reduction, is accomplished with success using this filter.

a)

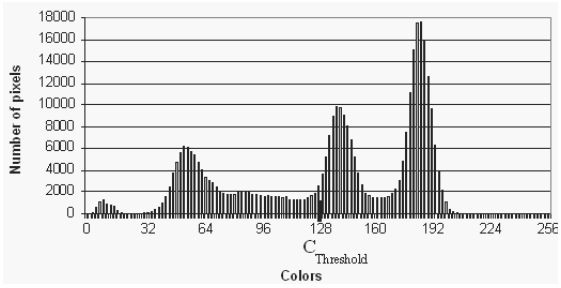

b)

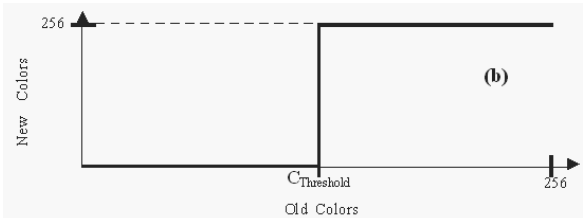

Fig. 8. Intensity modification to identify two-color zones: a) histogram of the color distribution with the threshold factor, b) color conversion

It is necessary to carry out a second intensity modification to distinguish the two zones in the image (the solid substrate and the liquid drop). Similar to the first modification, again using the histogram of the colors, the threshold factor ($C_{threshold}$) is assigned a value equivalent to the middle value of the histogram as shown in Figure 8a [10]. Using this value, a threshold filter is applied (Figure 8b). This factor can be adjusted for each experiment by the user through the user interface. By default, this coefficient is set to 50 percent for the middle value.

3.2. Outline detection

An outline can be defined as a pixel situated at the border of an abrupt variation of intensity. A pixel can be named as an outline by comparing with the intensities of the surrounding pixels which are defined as the east, west, north, and south neighbours (see Figure 9a). In this Figure, C_{ij} is the color of the pixel of interest and $C_{(i+1)j}$, $C_{(i-1)j}$, $C_{i(j-1)}$ and $C_{i(j+1)}$ are the corresponding colors for the east, west, north, and south neighboring pixels, respectively. To make the algorithm more flexible, a set point parameter, SP, is added. This is a control parameter which is used to decide if the variation is abrupt enough or not. Given that the set point parameter is positive, the absolute value of each variation should be compared with this value (see Figure 9b). In see Figure 9c, the comparison of these calculated variations is shown schematically. If, at least, one of these calculated variation values exceeds the given value of the set point parameter, the pixel, whose color is defined as C_{ij}, is marked as a point that defines the outline. Afterwards, this procedure is repeated for each pixel of the image to find all of the points forming the outline.

a)

	C_{ij-1}	
C_{i-1j}	C_{ij}	C_{i+1j}
	C_{ij+1}	

b)

$$V_1 = \left| C_{ij}-C_{(i-1)j} \right|$$

$$V_2 = \left| C_{ij}-C_{(i+1)j} \right|$$

$$V_3 = \left| Cij-C_{i(j-1)} \right|$$

$$V_4 = \left| Cij-C_{i(j+1)} \right|$$

c)

If $V_1 > SP$ or
$V_2 > SP$ or
$V_3 > SP$ or
$V_4 > SP$, then
C_{ij} is an outline

Fig. 9. Outline detection algorithm: a) neighboring pixels, b) calculation of intensity differences, c) conditions for a pixel to be identified as outline

3.3. Pattern recognition

At this stage, a large quantity of raw information is available. It is already known which pixels form the outline; however, there is no link between the outline pixels and their corresponding patterns. It is important to note that only two patterns for two components (the sessile drop and the substrate) are of interest. A verification is carried out to see if the pixels identified as the outline are also part of these two components. To simplify this verification, a group of coordinates are entered. The desired zone of the image stays within this user defined region. The user enters the necessary coordinate information into the program by using the "analysis window" box which is found under the Config drop down menu of the program. Then, the detection of patterns and their assignment to the corresponding outline pixel are carried out only in this "analysis window".

The algorithm for the pattern identification uses an iterative method along a predefined research-axis. This axis can be characterized by its vertical or horizontal orientation and its length. The steps of this algorithm is as follows: For each point on the research-axis, the number of outline pixels found in the proximity of an axis that is orthogonal to the research-axis is found and placed in a histogram. In addition, only the pixels nearest to the orthogonal axis are counted.

As shown in Figure 10a, the "analysis window" is superimposed on the image to be analyzed. Figure 10b shows how the outline pixels are counted for each point of the histogram. Figure 10c presents the histogram obtained at the end of the search. At the end, the element of histogram which has the greatest number of points is associated with the upper part of the solid substrate. To reconstitute the pattern, it is sufficient to reuse the algorithm by taking this line as the root of the pattern and by grouping the points closest to the orthogonal axis in a data structure. This results in a table containing the coordinates of the pixels of the first symbol as shown Figure 10d. This algorithm finds linear patterns efficiently. But it is necessary to adapt the algorithm to the cases where the patterns are not linear.

The circular part of the image represents the second pattern to be identified, which is obviously not linear. This part of the image is divided into two halves by the vertical y-axis. The search is carried out for each half separately. Then, the utilization of the algorithm described above is possible with some modification. In the modified algorithm, the orthogonal axis moves to the same location as the actual point. At the same time, the research zone in the proximity of orthogonal axis is changed. The point which is closest to the orthogonal axis is added to the pattern as shown in Figure 10e. This point becomes the root of the orthogonal axis for the next iteration.

3.4. Pattern interpolation

A numerical method was incorporated into the analysis to perform a spatial transformation on the patterns. This transformation is necessary because the points obtained using the side detection algorithm introduces fluctuations into the derivative curves of the patterns. It is important to check if the information provided for the interpolation algorithm is coherent. Therefore, the first step in this stage is to filter the points forming the patterns. Once the points are filtered, an interpolation is done using the cubic spline algorithm [21].

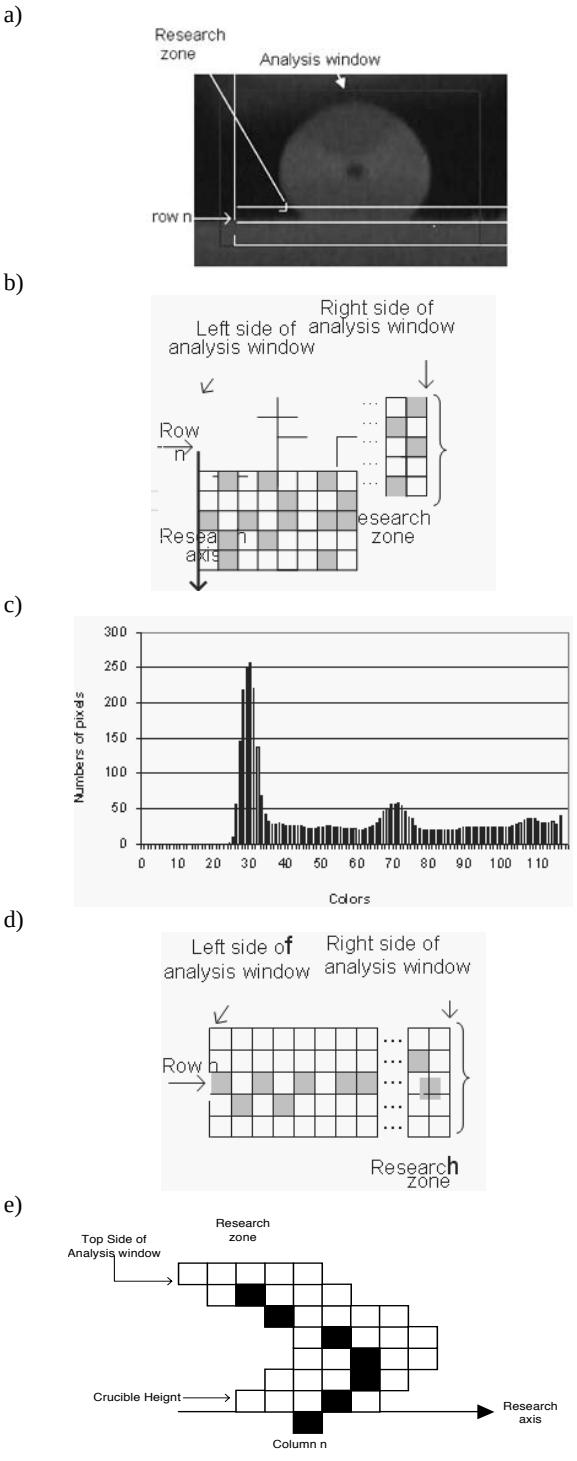

Fig. 10. Pattern recognition algorithm: a) original image with analysis window adjusted (linear component), b) research zone for the compilation of pixels in a specific row i. (linear component), c) histogram of all the lines on the research axis (linear component), d) resulting pattern of the selected line (linear component), e) case for non-linear components

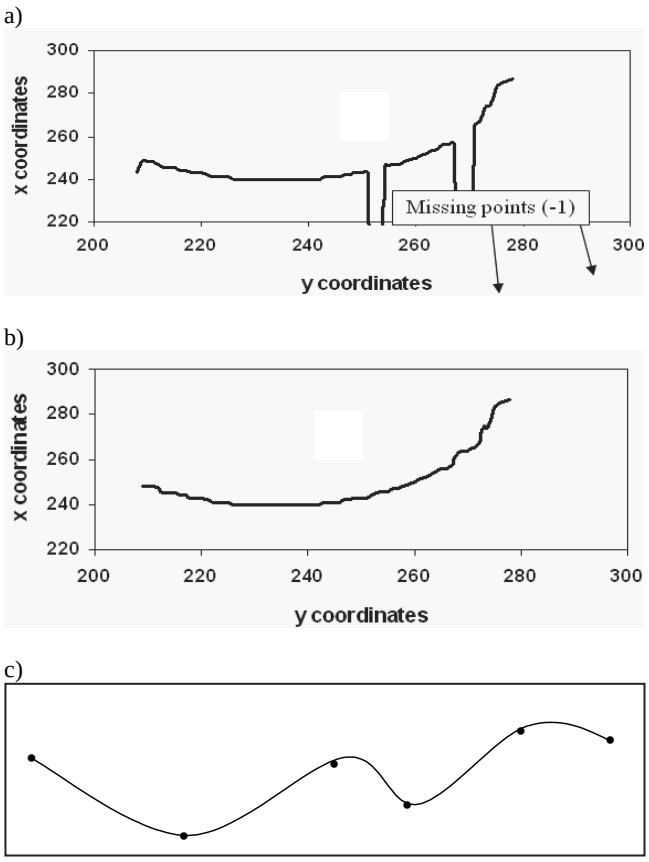

Fig. 11. Series of points forming the second pattern sight according to the research orientation: a) with the missing points (marked with negative values), b) as prepared for cubic spline interpolation, c) interpolation by cubic spline

The algorithm for the pattern recognition used is versatile; it is also capable of taking care of the missing outline points. These points are marked with negative values. The first step of the pattern filtering is to replace the negative values by carrying out a linear interpolation between the neighbouring points. An example of an outline with missing values is shown in Figure 11a. The effect of the two points with negative values is clearly seen. After the linear interpolation, the pattern takes the modified form show in Figure 11b.

After filtering, a cubic spline interpolation is carried out for the spatial transformation of the pattern. This algorithm approximates the curve between the referential points, as shown in Figure 11c. To generate a new pattern with the help of this transformation, only some points of the original pattern need to be transferred to the cubic spline module. One advantage of this algorithm is that the pattern generated (based on the referential points) is smooth.

Another advantage is the automatic calculation of the first and second derivatives. Then, it is possible to proceed with the analysis of the curves. After several verifications, it was seen that the proposed numerical method with the incorporated spatial

transformation improved both the detection of the droplet and the accuracy of the numerical values.

3.5. Linear regression

In this phase, it is very important that the algorithm carries out the following two steps with the highest precision. The first one is to find the slope at the starting point of the pattern. This is used to determine the angle at the intersection of the droplet and the solid surface. The second one is to find the point of reference needed to determine the dimensions of the drop which are then used in the surface tension calculation (see Figure 2). The latter is obtained from the first derivative of the droplet pattern. However, the derivative curve still has fluctuations as shown in Figures 12a and 12b. These fluctuations are caused by the discrete nature of the points involved.

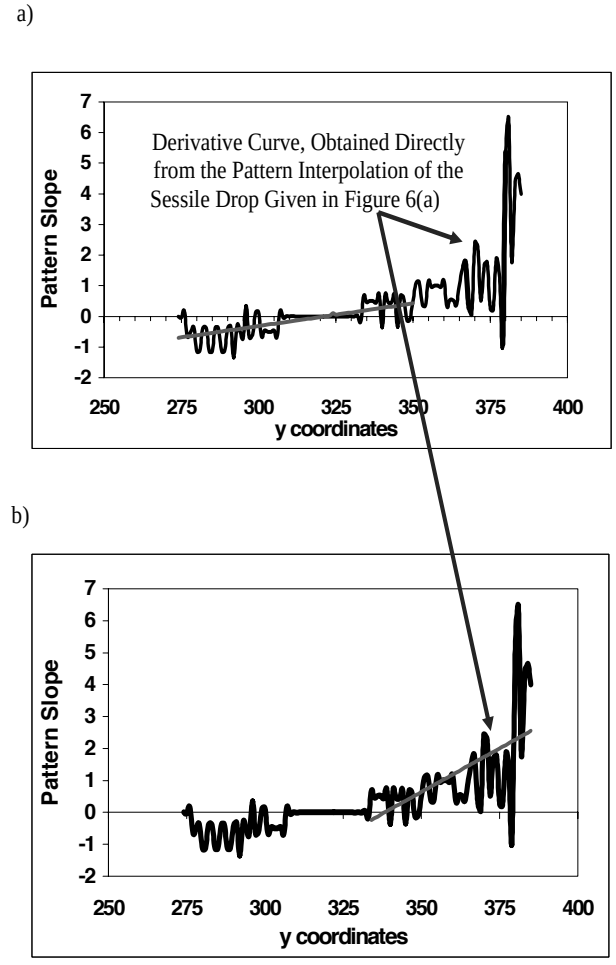

Fig. 12. Application of linear regression to: a) first section of a derivate curve to determine the slope at the droplet-crucible intersection, b) last section of a derivate outline to determine the stress surface parameter

The droplet/crucible intersection is located on the left side of the discontinuity observed on the derivative curve. Therefore, the initial slope of this section of the curve is estimated by a linear regression [21] as shown in Fig. 12a. As it can be seen from Figure 2, some of the dimensions used in surface tension calculations (H, H', and h) are determined from the vertical line passing through the drop and intersecting the 45° line (slope equal to 1) that is tangent to the drop contour. Determining the point where the derivative is equal to one is difficult because of the fluctuations. Therefore, the software also carries out a linear regression [21] over the end section of the derivate curve as shown in Figure 12b. The linear regression approximation provides a reliable value of the derivative. Further refinement to this method could be developed based on a non-linear interpolation.

3.6. Calculations

To calculate the area of the circular pattern, a numerical integration is used. It is to be noted that, for the circular pattern, two series of coordinates are available (one for each side of the y-axis). The differences between the x-coordinates (for a given y coordinate or height) on both sides of the circular pattern are calculated. This gives the width of the circular pattern at different heights. The width is multiplied by the scaled metric width of a pixel. Then, this value is also multiplied by the metric height of the pixel to calculate the area at a specific droplet height. To find the total area, the sum of all rectangles is calculated from the following equation:

$$\boldsymbol{Area} = \sum_{Y=Y_{\min}}^{Y_{\max}} ((X_2(Y) - X_1(Y)) \cdot \boldsymbol{W_{pixel}}) \cdot \boldsymbol{H_{pixel}} \tag{2}$$

where X_2 and X_1 are functions that call the right and left coordinates of the circular pattern for a height "Y" in the image. W_{pixel} and H_{pixel} are the width and the height of a pixel, respectively.

For the volume calculation, always using the coordinates of the circular pattern, the volume of each disc located at a height Y is calculated. Thus, the volume of the drop which is the sum of all disc volumes is given by:

$$\boldsymbol{Volume} = \sum_{Y=Y_{\min}}^{Y_{\max}} \pi \left[\frac{(X_2(Y) - X_1(Y)) \cdot \boldsymbol{W_{pixel}})}{2} \right]^2 \cdot \boldsymbol{H_{pixel}} \tag{3}$$

For the determination of the contact angles, it is necessary to calculate the slope of the two vectors at each point of intersection. The linear regression is used to calculate the slopes at these reference points for each pattern because of the presence of noise. Once the vectors are found, the angle (β) between the two vectors ($\vec{V}_1, \vec{V}_2$) is found using the following equation which is derived from the relation for a scalar product:

$$\beta = \cos^{-1} \frac{\vec{V}_1 \bullet \vec{V}_2}{\left|\vec{V}_1\right| - \left|\vec{V}_2\right|} \tag{4}$$

4. Wetting case

In the case of wetting, the contact angles are smaller than 90° on both sides of the drop. This situation is not compatible with the algorithm described above. To be able to determine the contact angles when the liquid starts to wet the surface of the solid, a new root detection algorithm has been incorporated into the analysis pipeline. This new algorithm is executed when the roots of the circular component cannot be found with the regular root detection algorithm.

In this case, the nature of the solid substrate pattern makes it impossible to find the roots because this pattern contains the information for the circular component in its data structure.

Fig. 13a shows such a solid substrate pattern. When the contact angle is smaller than 90°, the drop border (roots) is found for this pattern. Then, it becomes simple to generate the circular component from these two roots.

The root finding algorithm uses the first derivative of the solid substrate pattern. Figure 13b shows the derivative. It can be seen from this figure that the roots are located near the highest and lowest values of the derivative. More precisely, the roots are situated between the last reference point of the solid substrate (derivative ≈ 0) and the highest or lowest derivative value. The roots are then defined at a distance ±d from these reference points.

a)

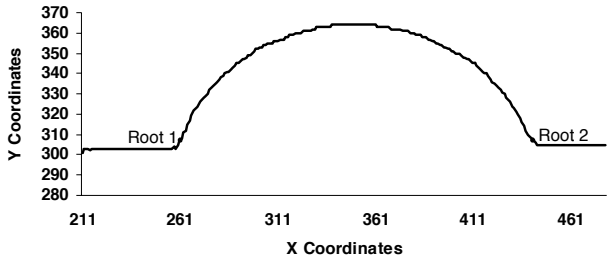

b)

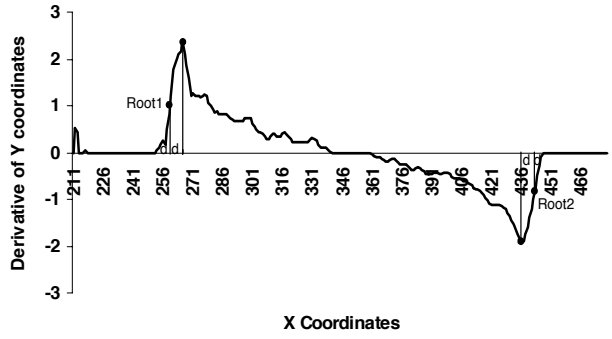

Fig. 13. Solid substrate pattern in a wetting case: a)spatial curve, b) derivative of the spatial curve

After the roots are defined, the circular component is generated. The first half of information between the two roots represents the left side of the drop and the second half of information represents the right side of the drop. Once, the left and right sides of the circular component are determined, the calculation module of the analysis pipeline can extract the information on the solid substrate pattern.

5. Results

The software was tested for both wetting and non-wetting systems as well as for an irregular drop. Aluminum and its alloys do not wet alumina as seen in Figure 6a. For this system, alumina was in granular form; consequently, the surface of the solid was very rough. The experimental results showed that the pinning effect of the surface roughness on the contact angle is quite dominant. All the angles measured were similar and around 120°. The liquid drop is pinned down by the rough edges of the alumina particles which prevented the drop from spreading and taking its proper form.

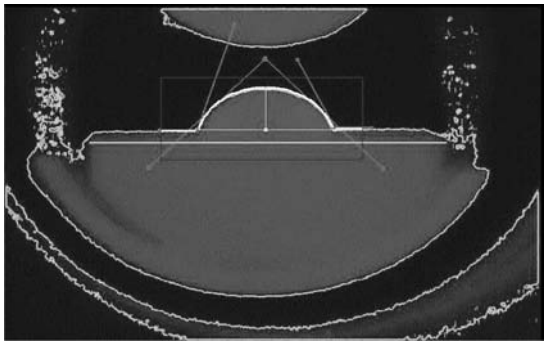

Fig. 14. Software output showing the outline determination, measurement of angles, and other geometric parameters for the wetting case shown in Fig. 6b (Green lines are the outline, blue line is the analysis window, red lines show angle detection and 45° angle, see Fig.)

Fused silica and Al-7wt%Mg alloy form a wetting system Figure 6b. Figures 14 present the image treated by the image analysis software developed for this system. The analysis window along with the lines which are used for determining the angles and the geometric parameters is shown. As can be seen from this figure, the contact angles are determined on both sides of the drop.

The change in the contact angle with time for the molten alloy drop on the solid fused silica obtained from a series of images using this software can be seen in Figure 15a. In this figure, the angles measured on both sides of the drop as well as their averages are presented. As it can be seen from this figure, the contact angle seems to be decreasing with time which indicates an increase in wetting.

In theory, if the solid substrate surface is perfectly smooth, rigid, chemically homogenous, and perfectly horizontal on the x-axis, the same contact angles should be measured from both sides. Although these conditions are valid for the fused silica substrate (whose image is given in Figure 14, the contact angles measured from the two sides are slightly different. This error stems from

mainly two sources: (i) the roughness of the substrate and (ii) the unfavourable characteristics of aluminium and magnesium alloys at high temperatures.

The fused silica substrate is polished down to 4 Å [24]. Since their effective roughness values are quite low for this study, they are considered to be smooth for the wettability studies. However, even such a low roughness causes an error during the contact angle measurements [9].

The second factor, which is considered as a source of error in the contact angle measurements, is the oxidation of the sessile drop some time after it is formed on the solid substrate. Oxidation does not contribute to the measurement errors at the beginning of the experiment because the measurements are carried out immediately following the sessile drop formation. However, as the time progresses, the surface of the aluminum drop is oxidized despite the precautions taken to minimize the presence of oxygen in the system. This oxide layer does not allow the sessile drop to change its shape freely if chemical wetting (for example, spinel formation) is taking place at the solid/liquid interface [12]. Also, the vaporization of magnesium present in the alloy further complicates the situation. Figure 15 (b) presents the change in the spreading (S) and the maximum drop diameter (d_m) with time; and Figure 15c shows the change in parameters H and H' with time. The changes in the drop surface and volume with time are shown in Figure 15d. The spreading and the maximum diameter data coincide because, for this case, the maximum diameter is located at the bottom of the drop. All these three figures indicate that the drop becomes smaller as the time passes which is probably due to the magnesium evaporation and the deformation in the drop shape with oxidation. Therefore, as far as the aluminum alloys are considered, the sessile-drop technique should be used to measure the initial wettability only. However, the software can be used for other solid-liquid systems. The surface tension calculated using the initially measured parameters is 0.5 N/m which is lower than its reported value of 0.58 N/m in literature [20] for Al-7wt%Mg alloy in argon atmosphere. However, it should be noted that the reported values of surface tension for aluminum and its alloys vary significantly in the literature due to the measurement difficulties and unavoidable oxidation.

In Figure 16a, the original image of a sessile drop that is exposed to extreme oxidizing conditions is given. Its shape becomes irregular because of oxidation. When a sessile drop is formed on layers of granular particles that are superposed loosely on one another, the level of the solid on the right hand side may be different than the one on the left hand side of the drop. This complicates the situation further for most of the other image analysis programs, but the current program addresses such situations as well: The yellow line shows the upper limit of the sessile drop (see Figure 16b); and as seen in this figure, the program takes this part of the sessile drop as a flat surface. The program is not able to fit a spline to the upper limit. However, it fits the spline up to a certain point, then assumes the drop is flat, and connects the last two points determined from each half. Obviously, some of the parameters will not be calculated correctly, but it will not fail to determine the contact angle values. In contrast, many programs using the Laplace's equation fail because it is not a condition dictated by this mathematical equation. In reality, however, such conditions exist. For instance, if a sessile drop is big enough, it will have a flat upper boundary due to the effect of gravity. The algorithm developed works even for such difficult condition. In Figure 16c, the measurements carried out manually by using the optical microscope are shown.

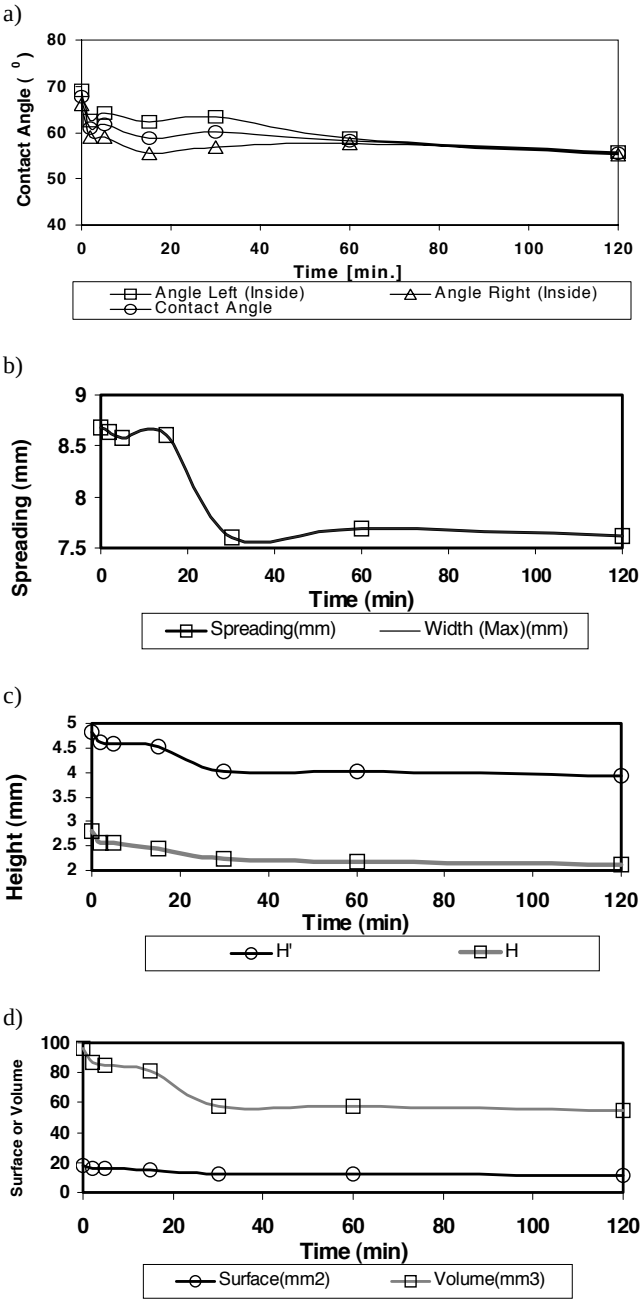

Fig. 15. Measurements done with the image analysis software for the wetting case shown in Figure 6b (Al- Mg alloy on fused silica) (a) contact angle (θ), (b) spreading (s) and maximum width of the drop (d_m), (c) H and H′ (Fig.), (d) surface and volume of the drop

a)

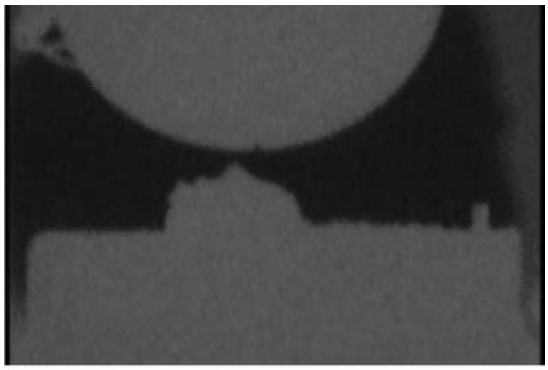

b)

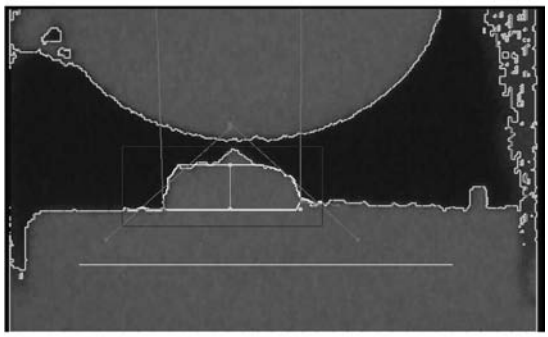

c)

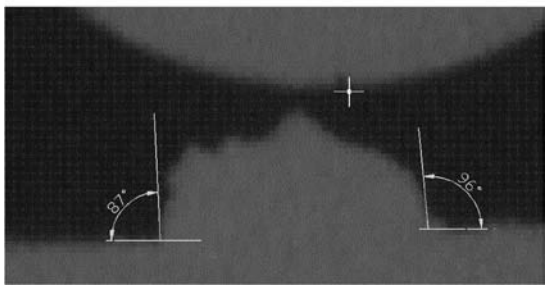

Fig. 16. Measurements carried out on an irregular image: a) raw image from the experiment, b) image outline and contact angles determined by the image analysis program, c) contact angles measured manually with the optical microscope

In addition, the contact angles measured using the image analysis software are validated by comparing them with those measured with the optical microscope. The results are given in Table 1.

Since the measurements are carried out by manually, each contact angle is measured 5 times and an average value is taken to minimize the error introduced by the user of the microscope. In this table, the contact angle values for three images are given. Two of them are the examples given in Figure 6 for wetting and non-wetting systems, and the third one is the example given for the oxidized sessile drop with an irregular shape. From this Table, it can be seen that the optical microscope and the image analysis program results are in good agreement for regular images. As far as the irregularly-shaped sessile drop is concerned, there is a slight, but acceptable difference between the results obtained from the image analysis program and the optical microscope measurements.

Table 1.
Summary of contact angles measured by the image analysis program and the optical microscope

	0 minutes	2 minutes	5 minutes	15 minutes
Al/Alumina (measured by program)	127.49	127.49	127.49	127.49
Al/Alumina (measured manually)	127.4	127.4	127.4	127.4
Al-Mg alloy/fused silica (measured by program)	69	70	71	69
Al-Mg alloy/fused silica (measured manually)	69.5	68.9	68.8	67.5
Irregular shape (measured by program)	93.2	93.2	93.2	93.2
Irregular shape (measured manually)	87.7	87.7	87.7	87.7

6. Conclusions

An image analysis software has been developed to determine the contact angle, surface tension, spreading, drop surface and the drop volume from the images obtained during the sessile drop experiments. The utilization of such a tool accelerates the analysis when a large number of images have to be treated. Depending of the quality of these images, the analysis produces the desired parameters with an acceptable accuracy. The results are validated by comparing them with the measurements conducted using an optical microscope; and the agreement is good. The image analysis software successfully gives the evolution of various parameters and contact angles with time. The experimental difficulties encountered in this work are due to the nature of aluminum-magnesium alloys. The software is able to measure precisely what the image shows.

To improve the success of the analysis, some of the parameters must be configured by the user through the interface. The analysis module is versatile, and it can be calibrated and adjusted to the series of images to be treated. The adjustment of the image contrast and the position of the analysis window are examples of parameters that can be configured specifically for a given set of images. Also, the system can be calibrated to give the measurements in SI units instead of pixels. This avoids the necessity of placing the camera at exactly the same position during each experiment.

The future work will cover the development of new filters which will eliminate further the interference of components placed outside the "analysis window" with the components to be analyzed. This task will have an impact at the level of filtration in the operation pipeline presented above.

Acknowledgements

Authors would like to thank NSERC, CQRDA, and FUQAC for the funding of the project.

References

[1] A.W. Adamson, Physical Chemistry of Surfaces, Wiley, New York, 1982.

[2] J.M. Alvarez, A. Amirfazli, A.W. Neumann, Automation of axysymmetric drop shape analysis-diameter for contact angle measurements, Colloids and Surfaces A-Physicochemical and Engineering Aspects 156/1-3 (1999) 163-176.

[3] E. Angel, Discrete Techniques in Interactive, Computer Graphics, Addison-Wesley, Reading MA, USA, 1997, 71-414.

[4] C. Atae-Allah, M.Cabrerizo-V'ılchez, J.F. G'omez Lopera, J.A. Holgado-Terriza, R. Rom'an-Rold, P.L. Luque-Escamilla, Measurement of surface tension and contact angle using entropic edge detection, Measurement Science and Technology 12/3 (2001) 288-298.

[5] F. Bashforth, J.C. Adams, An Attempt to Test the Theory of Capillary Action, Cambridge University Press, London, 1982.

[6] O.I. Del Rio, D.Y. Kwok, R. Wu, J.M. Alvarez, A.W. Neumann, Contact angle measurements by axisymmetric drop shape analysis and an automated polynomial fit program, Colloids and Surfaces A-Physicochemical and Engineering Aspects 143/2-3 (1998) 197-210.

[7] N.E. Dorsey, A new equation for the determination of surface tension from the form of a sessile drop or bubble, Journal of the Washington Academy of Sciences 18 (1928) 505.

[8] N. Eustathopoulos, M.G. Nicholas, B. Drevet, Pergamon Materials Series, Wettability at High Temperatures, Vol. 3, Pergamon, Oxford, 1999.

[9] B.M. Gallois, Wetting in nonreactive liquid metal-oxide systems, Journal of the Minerals, Metals and Materials Society 49/6 (1997) 48-51.

[10] R.G. Gonzalez, Digital Image Processing, Addison-Wesley, Reading MA, USA, 1992.

[11] Yu.A. Koshevnik, I.M. Kusakov, N.M. Lubman, Determination of surface tension of liquids from the dimensions of sessile drop, Russian Journal of Physical Chemistry A 27/12 (1953) 1887-1894 (in Russian).

[12] C.G. Levi, G.J. Abbaschian, R. Mehrabian, Interface interactions during fabrication of aluminum alloy-alumina fiber composites, Metallurgical Transactions A-Physical Metallurgy and Materials Science 9/5 (1978) 697-711.

[13] V. Leroux, J.C. Labbe, M.E.R. Shanahan, Contact angle and surface tension measurements on a metal drop by image processing and numerical calculations, High Temperature Materials and Processes 19/4 (2000) 351-364.

[14] L.E. Murr, Interfacial Phenomena in Metals and Alloys, Addison-Wesley Publishing Company, Reading, MA, 1975.

[15] A.W. Neumann, J.K. Spelt, Eds. Surfactant Science Series, Applied surface thermodynamics, Dekker, New York, 63, 1996.

[16] S.B.G.M. O'Brian, Wettability and Adhesion, Some Surface Tension and Contact Angle Problems in Industry, in Contact Angle, VSP Publishers, 1993, 937-951.

[17] M.E.R. Shanahan, Profile and contact angle of small sessile drops: a more general approximate solution, Journal of the Chemical Society, Faraday Transactions 1: Physical Chemistry in Condensed Phases 80/ 1 (1984) 37-45.

[18] A. Sklodowska, M. Wozniak, R. Matlakowska, The method of contact angle measurements and estimation of work of adhesion in bioleaching of metals, Biological Procedures Online 1/3 (1999) 114-121, (Available at: http://www.biologicalprocedures.com).

[19] D.N. Stacopolus, Computation of surface tension and of contact angle by the sessile drop method, Journal of Colloid and Interface Science 23/3 (1967) 453-458.

[20] K.R. Van Horn, Ed., Aluminum, Properties, Physical Metallurgy and Phase Diagrams, American Society of Metals, Park 1 (1967) 179.

[21] H. William, Interpolation and Extrapolation: Cubic Spline Interpolation and Modelling of Data: Fitting Data to a Straight Line in Numerical Recipes in C: The Art of Scientific Computing, Cambridge University Press 113-117 (1992) 661-666.

[22] R.P. Woodward, FTA200 Measurement Capabilities, 2007 (http://www.firsttenangstroms.com/pdfdocs/mea.pdf).

[23] http://www.omegamultimedia.com/products/media100/cinestream-win.htm

[24] The related departments of Stanford University approve the polishing procedures and guarantee the final roughness of the substrates.